Cellulose (2023) 30:3837–3852
https://doi.org/10.1007/s10570-023-05126-7

ORIGINAL RESEARCH

Thiol-functionalized chitosan poly(protic ionic liquids) hydrogel selectively anchors gold nanoparticles for aqueous catalysis

Lihua Zhang · Song Feng · Furong Huang · Bo Li · Yunqi Li · Hailiang Sheng · Lijie Hu · Songmiao Liang · Haibo Xie

Received: 22 October 2022 / Accepted: 28 February 2023 / Published online: 13 March 2023

Abstract Well-dispersed gold nanoparticles (Au NPs) anchored by polymeric three-dimensional hydrogels for catalysis have received great attention, especially in aqueous-phase catalysis. In this study, thiol-functionalized chitosan poly(protic ionic liquids) hydrogel (TCPPILH) is delicately designed and prepared as a selective support material to anchor Au NPs by taking advantages of Au-thiol chemistry and facile preparation of protic ionic liquids (PILs). The TCPPILH was successfully synthesized by a protonation reaction of chitosan with 3-mercaptopropionic acid (MPA) and mercaptosuccinic acid (MSA) in water, and followed by shaping in ethanol coagulation bath via solution-gelation transition, and the properties can be facilely adjusted by changing the feed ratio of MPA and MSA. It is found that the TCPPILH can act as a selective support for adsorption of Au^{3+} ions, and a maximal anchoring capacity for Au NPs could reach up to 151.5 mg/g. The as-prepared TCPPILH@Au NPs catalysts were systematically characterized by FTIR, XPS, SEM, TEM, XRD and ICP-OES analysis, and the findings demonstrated that the TCPPILH could effectively inhibit the agglomeration of Au NPs (ca. 4.20 nm in diameter). As a proof of concept, hydrogenation of water pollutes, such as 4-nitrophenol and azo dyes with $NaBH_4$ as reductant was selected as model applications, and the results indicated that TCPPILH@Au NPs catalysts exhibited high catalytic activity and satisfactory reusability.

Supplementary Information The online version contains supplementary material available at https://doi.org/10.1007/s10570-023-05126-7.

L. Zhang · S. Feng · F. Huang · B. Li · Y. Li · H. Sheng · H. Xie (✉)
Department of Polymer Materials and Engineering, College of Materials and Metallurgy, Guizhou University, Guiyang 550025, China
e-mail: hbxie@gzu.edu.cn

L. Hu · S. Liang
Separation Membrane Materials and Technologies Joint Research Centre of Vontron-Guizhou University, Vontron Technol Co Ltd, Guiyang 550018, China

Graphical abstract

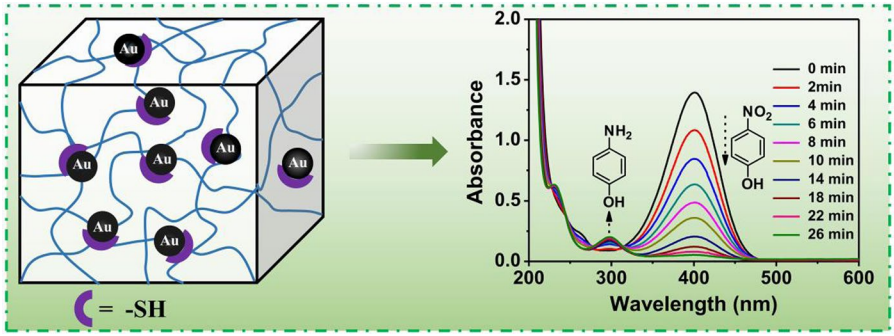

Thiol-functionalized chitosan poly(protic ionic liquids) hydrogel (TCPPILH) was delicately designed and prepared as a selective support material to adsorb Au^{3+} and anchoring Au NPs by taking advantages of Au-thiol chemistry and facile preparation of protic ionic liquids (PILs). This TCPPILH@Au NPs catalysts exhibited desired catalytic activity for the hydrogenation of 4-nitrophenol and azo dyes in water.

Keywords Chitosan · Poly(protic ionic liquids) hydrogel · Au nanoparticles · Au-thiol chemistry · 4-nitrophenol · Azo dyes

Introduction

Noble metal nanoparticles as catalysts have found broad applications in hydrogenation/dehydrogenation, oxidation, coupling reaction and so on (Bratlie et al. 2007; Jiang et al. 2011; Wang et al. 2019; Wei and Chen 2012). Specifically, gold nanoparticles (Au NPs), representing a relevant example of noble metal nanoparticles, have created growing interest in the catalysis area because of their superior catalytic activity (Miyamura et al. 2015; Zubair Iqbal et al. 2021). For example, Au NPs perform high catalytic activity for hydrogenation of nitrophenols and azo dyes in aqueous environment, and thus function as precious catalysts in terms of water environmental protection (Fu et al. 2019; Hong et al. 2022). However, there still remains agglomeration challenge due to the high surface energy of Au NPs, which usually leads to significantly reduced catalytic activity (Fu et al. 2019; Ilgin et al. 2019). Therefore, the design and preparation of rational supporting materials capable of inhibiting agglomeration and preserving catalytic activity of Au NPs have obtained much attention (Alle et al. 2021). Many studies have been carried out on the anchoring of Au NPs on supporting materials, such as graphene (Ventura-Espinosa et al. 2021), mesoporous silica (Yan et al. 2020), metal–organic frameworks (MOF) (Dhakshinamoorthy et al. 2017), and hydrogels (Jayaramudu et al. 2013). Among these materials, hydrogels have obtained particular interests, as their three-dimensional, hydrophilic network structure and high structural tunability not only provide cross-linked polymer network to host, disperse and stabilize NPs, but also provide an ideal environment especially for sustainable aqueous catalysis (Li et al. 2019; Thoniyot et al. 2015). It is believed that the particular molecular structure of hydrogel delivers significant correlations with the in situ adsorption and reduction of metal ions in the hydrogel, as well as inhibits the agglomeration of NPs during the preparation process and even the practical application (Li et al. 2019; Zhu et al. 2021). For example, with the use of tannic acid (a plant polyphenol), Au NPs decorated graphene hydrogel was successfully developed, and tannic acid aided in formation of hydrogel and also worked as reducing agent and stabilizer for Au NPs (Luo et al. 2015). Poly(*N*-isopropylacrylamide) (PNIPAM) hydrogels loaded with Au NPs presented a good temperature-controlled catalyst system for the reduction of 4-nitrophenol (4-NP) to 4-aminophenol (4-AP) (Marcelo et al. 2014). Therefore, innovated and elegant design of chemical molecular structure of hydrogels capable of anchoring Au NPs will

significantly promote the development of sustainable catalytic chemistry.

In the last years, Au-thiol chemistry is being highlighted for the relatively strong affinities (184 kJ/mol), which has proven to be an excellent strategy for selective adsorption of Au^{3+} ions and anchoring or stabilization Au NPs (Biswas et al. 2016; Nutan and Jewrajka 2020; Wang et al. 2017; Zhao et al. 2021). Several hydrogels containing thiol (-SH) or disulfide (S–S) groups have demonstrated their strong bonding feature with Au (Cao et al. 2010; Laomeephol et al. 2020; Lin et al. 2021). As an example, thiol-functionalized PNIPAM microgels were designed for incorporation of Au NPs, and the distribution of Au NPs within the microgels can be easily controlled by the distribution of thiol groups (Shi et al. 2013). Special attention should be given to a novel thioether-functionalized hydrogel prepared from the polymerization of acrylamide and *N*-methacrylamidothiomorpholine (MTM), which was used as a selective support material to anchor Au, demonstrating good catalytic activity for the reduction of 4-NP (Ilgin et al. 2019). Although significant progress has been achieved, these synthetic strategies to induce thiol chemistry into hydrogel still remain shortages, such as use of complex and expensive functional monomer containing sulfur element, and multi-step synthesis; therefore, the development of new synthetic protocol aiming a facile preparation of thiol-functionalized hydrogel for Au NPs catalysis is still an important research topic.

One of the important factors to construct hydrogel is the synthesis or selection of a hydrophilic crosslinked polymer matrix. Chitosan, the second most abundant polysaccharide after cellulose, has attracted much attention as raw material for constructing hydrogel networks (Ge et al. 2016; Liu et al. 2022; Tabassum et al. 2021). Notably, the structure of chitosan is featured by abundant amino and hydroxyl groups, offering great opportunities for anchoring metal NPs and post-modification for further functionalization to prepare chitosan-based materials with enhanced properties (Lasko et al. 1993; Liu et al. 2016; Wu et al. 2020; Zhao et al. 2014). For example, surface-functionalization of activated coke by chitosan was capable of anchoring and stabilizing Au NPs due to the surface-rich amino and hydroxyl groups of chitosan (Fu et al. 2019).

Ionic liquids (ILs) are generally recognized as organic liquid salts, consisting of organic cations and organic/inorganic anions, which have been widely used in green catalysis, electrochemistry, and functional material fields (Fabre and Murshed 2021). ILs can be distinguished into aprotic ILs (AILs) and protic ILs (PILs), and the PILs are easily formed by the proton transfer from a Brønsted acid to a Brønsted base (Li et al. 2019; Qian et al. 2017). If a particular functional group was introduced onto the ILs structure, a concept of task-specific ILs or functional ILs was proposed (Singh and Savoy 2020). For example, thiol-functionalized ILs have been prepared and immobilized on the Au electrode by the stable Au–S bond for electrochemical/electrochemiluminescence sensors (Chen et al. 2016). A class of poly(ILs) materials, featured by the pendant AILs or PILs on a polymer chain, have been proposed and prepared aiming to combine the polymer material properties and the unique properties of ILs (Qian et al. 2017). The design, preparation and application of poly(AILs) have obtained extensive concerns during the past decades (Qian et al. 2017). However, the design, preparation and application of poly(PILs) are still in fancy, although it can be facilely prepared.

As aforementioned, there are amount of amino groups in chitosan, indicating facile proton transfer reaction sites for the construction of PILs moiety onto chitosan by using various inorganic and organic acids (Cheng et al. 2019). While the design, preparation and application of poly(PILs) derived from chitosan by taking its inherent feature of amino groups structure is over-neglected, in comparison to poly(AILs). Particularly, there is no report in terms of chitosan-derived task-specific poly(PILs) materials. Herein, taking the structural features of chitosan and 3-mercaptopropionic acid (MPA) as well as mercaptosuccinic acid (MSA), a series of thiol-functionalized chitosan poly(protic ionic liquids) hydrogel (TCPPILH) were delicately designed and prepared via ionic crosslinking (Scheme 1). The TCPPILH presented outstanding performance in selective absorption of Au^{3+} ion and could stabilize and disperse Au NPs due to the presence of the thiol functional moieties in the hydrogel. Furthermore, the TCPPILH@Au NPs catalysts presented satisfactory catalytic performance in the reduction treatment of typical water pollutes under mild conditions.

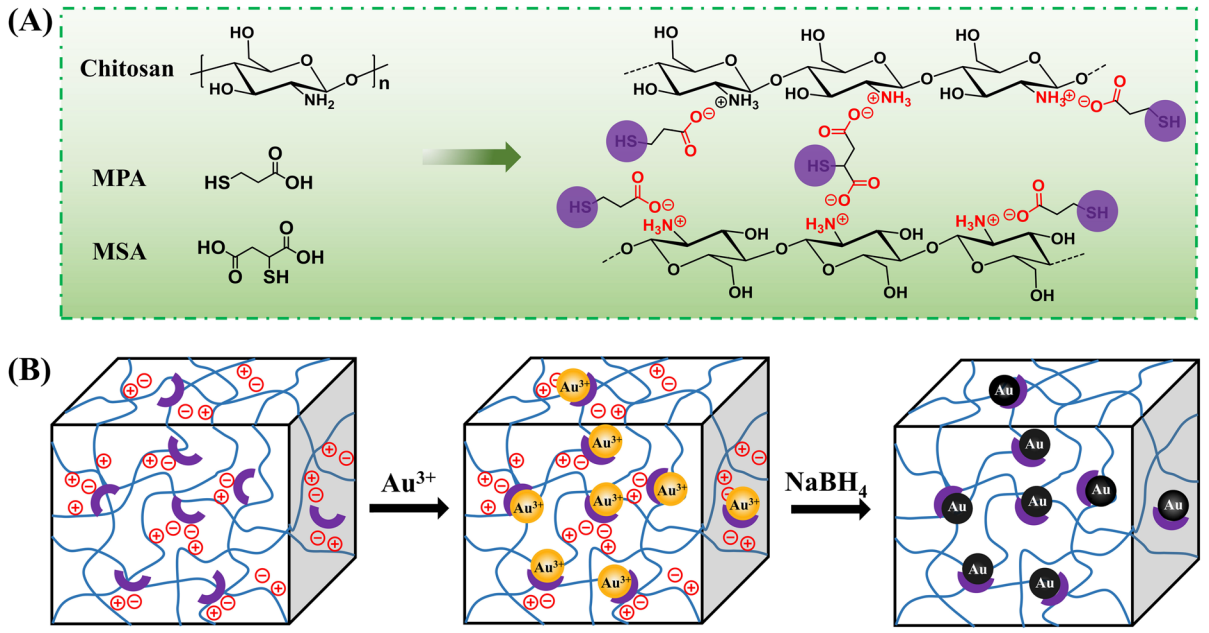

Scheme 1 **A** Mechanism of the formation of TCPPILH by using chitosan, MPA and MSA; **B** Schematic representation of the TCPPILH@Au NPs catalysts

Table 1 The formula for preparation of TCPPILH beads and the loading of Au NPs[a]

Sample	MPA (mmol)	MSA (mmol)	$n_{COOH(MPA)}$: $n_{COOH(MSA)}$	Anchored Au NPs (mg/g)[b]
TCPPILH-1	13.368	0	10:0	–
TCPPILH-2	10.694	1.337	8:2	–
TCPPILH-3	8.021	2.674	6:4	68.1
TCPPILH-4	6.684	3.342	5:5	151.5
TCPPILH-5	5.347	4.010	4:6	114.8
TCPPILH-6	2.674	5.347	2:8	93.8
TCPPILH-7	0	6.684	0:10	59.8

[a]chitosan (1.25 g), water (20 mL), dissolution temperature (80 °C), and dissolution time (6 h)

[b] "-" means the beads were too fragile to maintain structural integrity

Materials and methods

Materials

Chitosan (degree of deacetylation of 96.5%), mercaptosuccinic acid (MSA), 3-mercaptopropionic acid (MPA), 3-hydroxypropionic acid, DL-malic acid, sodium borohydride ($NaBH_4$), Congo red (CR), Erichrome black T (EBT) and methyl orange (MO) were provided by Aladdin Reagent Co., Ltd. The viscosity-average molecular weight of chitosan was calculated to be 6.6×10^5 g/mol, based on its intrinsic viscosity according to the Mark-Houwink-Sakurada equation (Kasaai et al. 2000; Tan et al. 2021). 4-Nitrophenol (4-NP) was supplied by Energy Chemical Co., Ltd. Sodium tetrachloroaurate (III) dihydrate ($NaAuCl_4{\cdot}2H_2O$) (Aladdin) was used as metal ion source. All chemicals were used as received.

Preparation of TCPPILH beads

The synthesis of TCPPILH beads with different amounts of thiol groups were carried out via a simple dropping method (Dong and Xiao 2017). Briefly, chitosan, MSA and MPA with the formula listed in Table 1 were added into deionized water, and the mixture was stirred under mechanical agitation at 80 °C for 6 h to complete the dissolution of chitosan. After centrifugation at 10,000 rpm, the degassed chitosan solution was injected to ethanol through a syringe needle. The droplets formed at the outlets because of surface tension and the capillary forces,

then the alcogel beads formed by the precipitation effect of ethanol. After solidification in ethanol for at least 12 h and then soaked in fresh deionized water, the as-prepared TCPPILH beads were preserved for further use.

Swelling properties of TCPPILH beads

The swelling ratio of the prepared TCPPILH beads was determined by a gravimetric method. The mass of fully swollen hydrogel beads after soaking in deionized water for 2 days (W_s), and the mass of dry beads after complete drying at 50 °C (W_d) were measured. Then the swelling ratio was determined based on at least ten hydrogel beads by using Eq. (1) (Nunes et al. 2017):

$$\text{Swelling}\ (\%) = \left[\left(W_s - W_d\right)/W_d\right] \times 100 \quad (1)$$

Preparation of TCPPILH@Au NPs catalysts

Fifty TCPPILH beads were immersed in 1.5 mM (50 mL) neutralized $AuCl_4^-$ aqueous solution for 12 h under gentle shaking. Then the hydrogel beads were rinsed with deionized water and immersed in 0.5 M (50 mL) $NaBH_4$ aqueous solution for 2 h. The obtained hydrogel beads anchoring Au NPs (expressed as TCPPILH@Au NPs) were separated and rinsed with water.

Adsorption of the TCPPILH beads for various metal ions were conducted in Ni^{2+}, Cu^{2+}, Co^{2+}, Pd^{2+} and Au^{3+} aqueous solutions (50 mL, 1.5 mM) by using 50 mg hydrogel beads, respectively. After $NaBH_4$ treatment, the amounts of anchored metal NPs were determined by inductively coupled plasma-optical emission spectroscopy (ICP-OES).

Catalytic procedures

The catalytic activity of the as-prepared TCPPILH@Au NPs catalysts for the hydrogenation of 4-NP was carried out using $NaBH_4$ as reductant. Typically, 0.5 mL of 4-NP aqueous solution (0.5 mM) and 2.5 mL of fresh $NaBH_4$ solution (0.1 M) were mixed in a quartz cuvette. Then the TCPPILH@Au NPs catalysts were added to start the catalytic reaction. UV–vis spectra of the mixture with time were recorded to track the reaction progress.

The apparent rate constant (k_{app}) values were determined by using Eq. (2):

$$\ln\left(C_t/C_0\right) = \ln\left(A_t/A_0\right) = -k_{app}t \quad (2)$$

where C_0 and C_t refer to the concentration of 4-NP at initial time and t time, respectively; A_0 and A_t refer to the absorbance ($\lambda = 400$ nm) at initial time and t time, respectively.

Activation energy (E_a) of the TCPPILH-4@Au NPs catalysts was also determined using the Arrhenius equation. Activation enthalpy ($\Delta H^{\#}$) and activation entropy ($\Delta S^{\#}$) were determined using the Eyring equation (Ilgin et al. 2019; Sahiner et al. 2010b):

$$\text{Arrhenius equation}: \ln k_{app} = \ln A - E_a/RT \quad (3)$$

$$\text{Eyring equation}: \ln\left(k_{app}/T\right) = \ln\left(k_B/h\right) + \Delta S^{\#}/R - \Delta H^{\#}/RT \quad (4)$$

where T is the absolute temperature, k_B is the Boltzmann constant (1.381×10^{-23} J/K), h is the Planck constant (6.626×10^{-34} J s), and R is the ideal gas constant (8.314 J/(K mol)).

In order to further confirm the catalytic activity of the TCPPILH@Au NPs catalysts, the catalytic hydrogenation of three typical azo dyes (MO, CR and EBT) were also conducted. Typically, 4 mg (dry weight) of TCPPILH@Au NPs catalysts were added into a mixed solution of 0.5 mL of dye aqueous solution (1.5 mM) and 2.5 mL of fresh $NaBH_4$ solution (0.1 M). UV–vis spectra of the mixture with time were recorded to track the reaction progress.

Characterization

The FTIR spectra were recorded on a Thermo Scientific Nicolet iS50 spectrometer, and the spectra were recorded using 32 scans over a 4000–650 cm^{-1} range. The X-ray diffraction (XRD) experiments were performed on a PANalytical X'pert Powder X-ray diffractometer. The patterns with CuKα radiation ($\lambda = 0.15406$ nm) at 40 kV and 30 mA were recorded in the region of 2θ from 5 to 70°. Thermogravimetric analysis was performed on a TGA instrument (STA 409 PC, Netzsch, Germany) in an atmosphere of nitrogen from room temperature to 800 °C at a

heating rate of 10 °C/min. The elemental analysis (C, H, N, S) was performed on a Vario EL Cube Elementar analyzer. The surface element composition was measured using a Thermo Scientific K-Alpha X-ray photoelectron spectrometer. The morphology of hydrogel beads was observed by scanning electron microscopy (SEM, JSM-7500 F, JEOL). The transmission electron microscope (TEM) analysis was carried out with a FEI Tecnai G2 F20 electron microscope. The UV–vis measurements were conducted on a Shimadzu UV-2700 UV/vis spectrophotometer. The metal amount adsorbed in the hydrogel beads was determined using Agilent 5110 ICP-OES. Prior to determination, the solid samples were treated by acid digestion assisted by microwave using aqua regia.

Results and discussion

Preparation of TCPPILH and TCPPILH@Au NPs catalysts

The study started with the successful dissolution of chitosan in a new 0.67 M MPA aqueous solution (molar ratio of $-NH_2$ of chitosan to –COOH is 1:1.8, TCPPILH-1 in Table 1). It was found that with the addition of chitosan under mechanical stirring at 80 °C for 6 h, a transparent and viscous solution was achieved, indicating the successful dissolution of chitosan. This was also further confirmed by a polarization optical microscope (POM), demonstrating the disappearance of crystalline structure of chitosan, as shown in Fig. 1A and B. With the new chitosan solution in hand, we subsequently extruded the solution (Fig. 1C) into ethanol through a syringe needle, and a gelation phenomenon occurred immediately. Regretfully, the attempt of using the pure MPA-chitosan solution for the preparation of satisfactory TCPPILH is not successful via the typical solution-gelation

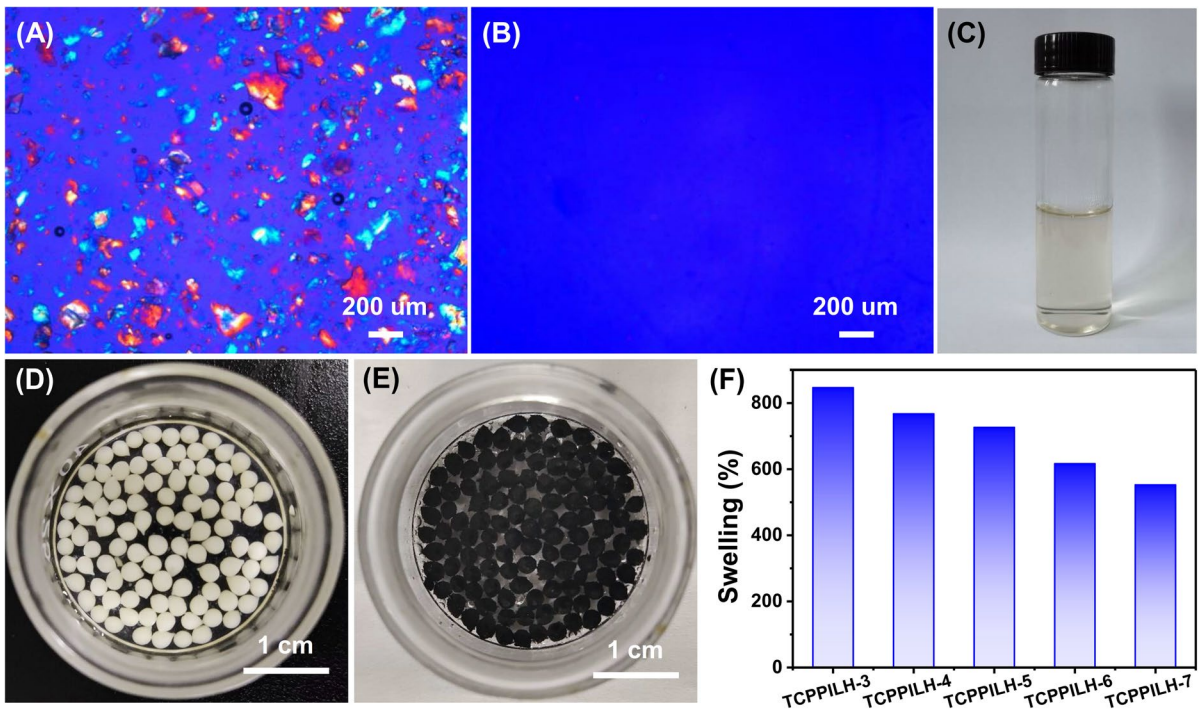

Fig. 1 Polarizing images of **A** chitosan suspended in MPA aqueous solution and **B** chitosan dissolved in MPA aqueous solution, pictures of **C** chitosan/MPA aqueous solution, **D** TCPPILH beads (TCPPILH-4) and **E** TCPPILH@Au NPs catalysts, and **F** swelling properties of TCPPILH-3 to TCPPILH-7

transition in ethanol and the TCPPILH-1 are too fragile to get self-supporting ability. The main reason is that the linear MPA and chitosan derived poly(PILs) is water-soluble. To our delight, with the increase in the molar ratio of MSA to MPA (Table 1), a series of TCPPILH beads were successfully prepared by the chitosan/MSA/MPA solutions, and the MSA could act as a crosslinker due to the ionic interactions between amino groups and the two carboxylic groups (Scheme 1), thus facilitating the formation of satisfactory gel. Regular spherical hydrogel beads with smooth surface and adequate structural integrity were achieved (Fig. 1D). It was found that at higher content of MSA, it was practically difficult to be handled to prepare TCPPILH-6 and TCPPILH-7 due to the high viscosity caused by a higher degree of crosslinking. Figure 1F shows the swelling properties of the TCPPILH beads, and the swelling ratio of TCPPILH-3 to TCPPILH-7 are determined to be 847% to 553%, respectively, indicating that the swelling ratio is significantly correlated with the crosslinking degree.

With the successful preparation of the TCPPILH beads, the rich content of thiol moieties in the gel stimulated us to identify their Au anchoring capability. The addition of TCPPILH into neutralized $AuCl_4^-$ solution under gentle shaking and followed by washing with deionized water and reduction with $NaBH_4$ solution achieved TCPPILH@Au NPs catalysts. This process was associated with the color change from white (Fig. 1D) to black (Fig. 1E). The EDS spectra of TCPPILH-4@Au NPs illustrate that the Au NPs are not homogeneously distributed in the hydrogel beads; that is, a negative gradient of the amount of anchored Au NPs exists from the surface to the interior of the hydrogel beads (Fig. S1). The whole content of the anchored Au NPs in the TCPPILH based on at least thirty dried beads were determined by ICP-OES, and the results are shown in Table 1. It was found that the loading amount of Au NPs are 68.1, 151.5, 114.8, 93.8 and 59.8 mg/g for TCPPILH-3, TCPPILH-4, TCPPILH-5, TCPPILH-6 and TCPPILH-7, respectively, indicating that the amount of anchored Au NPs highly correlates to the feed ratio of MPA and MSA in the preparation of TCPPILH beads. The initial increasing and then decreasing tendency of the Au content in the TCPPILH with the increase in molar ratio of MSA to MPA demonstrates the synergetic effect of crosslinked hydrogel network and the content of thiol moieties on the anchoring capability to Au. To further demonstrate the important role of thiol moieties in the hydrogel, a hydrogel similar to TCPPILH-4 was prepared by using chitosan, 3-hydroxypropionic acid and malic acid (chemical structure, Fig. S2), and it was found that the loading capacity of Au NPs by this hydrogel is only 3.5 mg/g (Fig. 2A). These

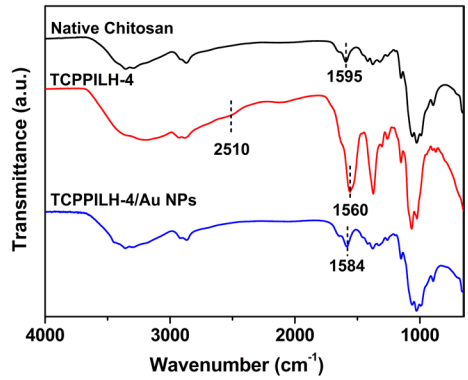

Fig. 3 FTIR spectra of native chitosan, TCPPILH-4, and TCPPILH-4@Au NPs catalysts

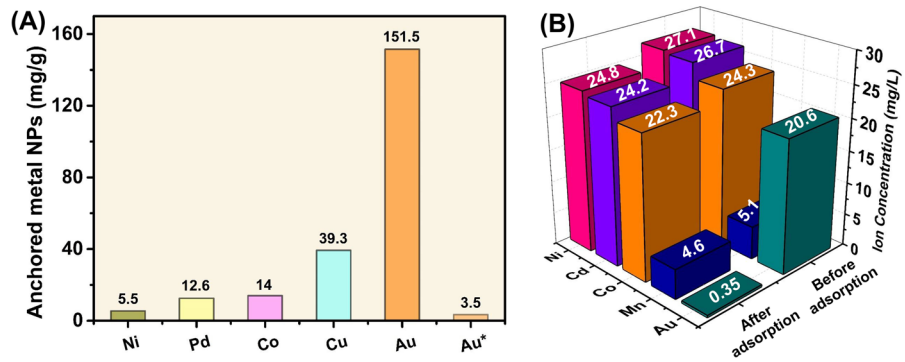

Fig. 2 **A** The anchoring amount of TCPPILH-4 for different kinds of metal NPs. The last column (Au* column) represents the Au NPs anchoring amount for a similar chitosan hydrogel prepared by 3-hydroxypropionic acid and malic acid. **B** Selective adsorption of $Au.^{3+}$ from a laboratory mimicked wastewater by TCPPILH-4

comparative results further indicate that the high loading amount of Au NPs mainly results from the strong Au–S bonding between gold and thiol groups in the hydrogel beads (Laomeephol et al. 2020; Lin et al. 2021; Wang et al. 2017).

It is also found that the TCPPILH has specific anchoring capacity to Au, which is evidenced by the low anchoring capacity of TCPPILH-4 to Ni, Cd, Co and Mn NPs (Fig. 2A). The selective adsorption experiment was further carried out by using a laboratory mimicked wastewater containing Au^{3+}, Ni^{2+}, Cd^{2+}, Co^{2+} and Mn^{2+} ions (Zhao et al. 2019a, 2019b). As shown in Fig. 2B, it can be observed that the TCPPILH-4 hardly adsorbs the coexisting ions, while almost all Au^{3+} ions can be adsorbed. This is attributed to the stronger affinity of gold ions with S and/or N on TCPPILH-4 than other kinds of ions. The findings demonstrate the potential of this TCPPILH for Au enrichment from industrial waste water and metallurgical industry (Zhao et al. 2019a, 2019b). These results also further confirm the strong driving force of Au-thiol chemistry in the preparation of TCPPILH@Au NPs catalysts.

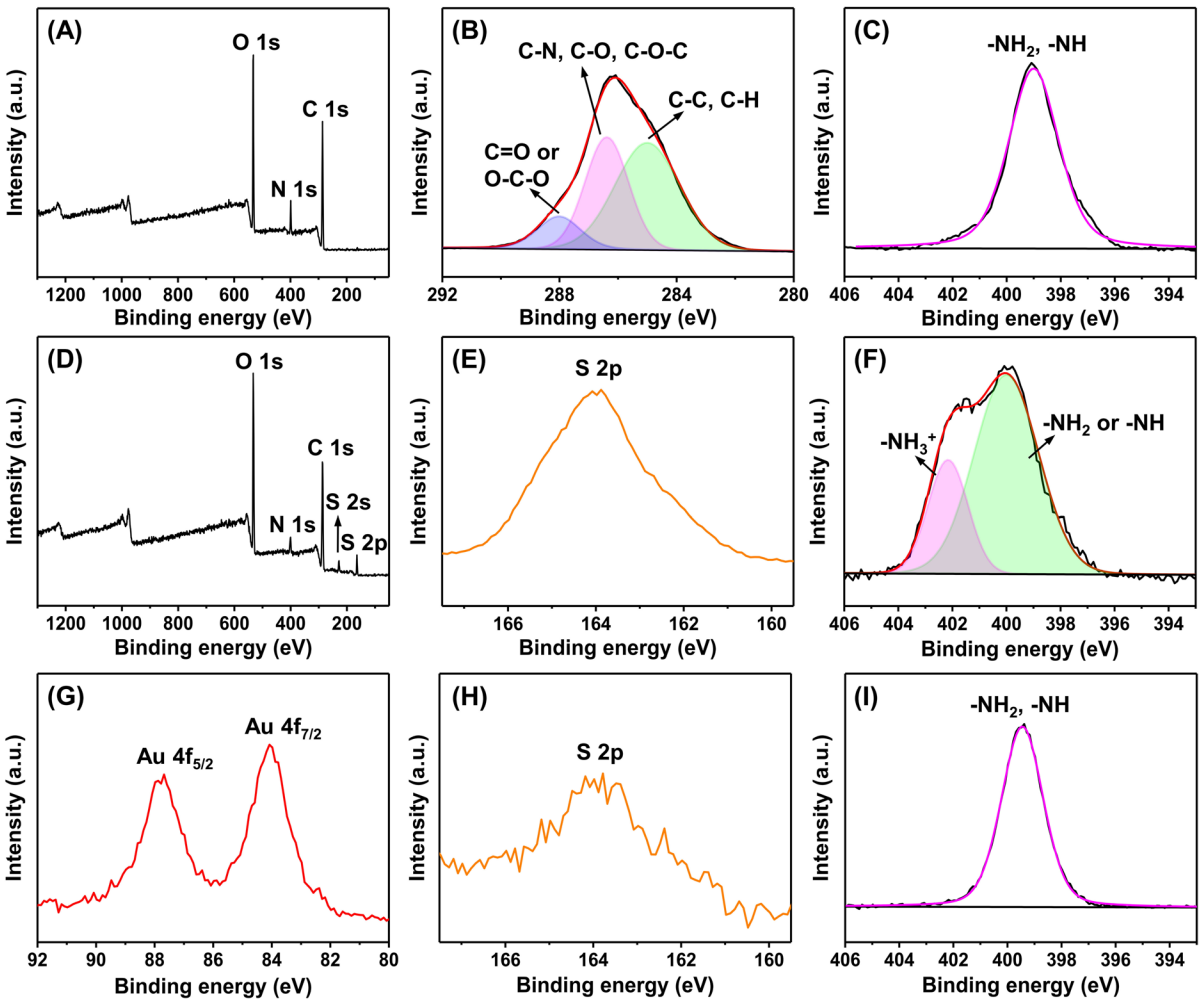

Fig. 4 **A** XPS full scan spectrum, high resolution spectra of **B** C 1 s and **C** N 1 s of native chitosan; **D** XPS full scan spectrum, high resolution spectra of **E** S 2p and **F** N 1 s of TCPPILH-4 beads; high resolution spectra of **G** Au 4f, **H** S 2p and **I** N 1 s of TCPPILH-4@Au NPs catalysts

Characterization of TCPPILH and TCPPILH@Au NPs catalysts

The structure evolution is clearly indicated by the FTIR spectra (Fig. 3). For TCPPILH-4, the peak at 1595 cm^{-1} assigning to N–H stretching of amino groups for native chitosan disappears, and the strong band of carbonyl stretching vibration at about 1700 cm^{-1} of MPA and MSA (Fig. S3) is also absent. And the newly formed peak at 1560 cm^{-1} can be attributed to the overlapped band between the asymmetric deformation of $–COO^–$ and the variable angle vibration absorption of $–NH_3^+$ (Ghosh et al. 2014). The minor peak at 2510 cm^{-1} can be assigned to the symmetric stretching vibration of –SH. These results indicate the successful preparation of cross-linked polymer matrix via protonation reaction between chitosan, MPA and MSA (Huang et al. 2007). The spectrum of TCPPILH-4@Au NPs indicates that the band intensity assigning to MPA and MSA decreases, indicating the leaching of MPA and MSA during the NPs preparation process due to the basicity of $NaBH_4$ aqueous solution, which destroyed the electrostatic interactions between chitosan, MPA and MSA. This is also evidenced by the element analysis results, showing that the S element is 6.27% in the TCPPILH-4, and 0.71% in TCPPILH-4@Au NPs (Table S1). Direct treatment of TCPPILH-4 with $NaBH_4$ aqueous solution achieved similar results (Fig. S4). In addition, for the TCPPILH-4@Au NPs sample, the slight blue shift of N–H stretching of amino groups from 1595 (native chitosan) to 1584 cm^{-1} (TCPPILH-4@Au NPs) implies the interaction between N atoms and Au NPs.

XPS analysis was further conducted to characterize the chemical constitution of native chitosan, TCPPILH-4 and TCPPILH@Au NPs (Fig. 4). It can be seen that only C, O and N exists in native chitosan (Fig. 4A). The high resolution C 1 s spectrum of native chitosan can be deconvoluted into three types of carbon species (Fig. 4B), including 285 eV (C–C and/or C–H bonds), 286.4 eV (C–N, C–O and/or C–O–C bonds), and 288.0 eV (O–C–O and/or C=O groups in residual chitin-like rings) (Kang et al. 2010; Zhao et al. 2019a, 2019b). And there is only one single N 1 s peak at 399.5 eV in the N 1 s spectrum of native chitosan (Fig. 4C). For the TCPPILH-4 beads, C, O, N and S exist in the full scan spectrum (Fig. 4D). The binding energy of S 2p bands at 164.0 eV (Fig. 4E) is close to the reported values (Castner et al. 1996; Laiho et al. 2003). The N 1 s peak (Fig. 4F) exhibits two peaks: 400.0 eV corresponding to neutral N in the forms of $–NH_2$ and/or –NH groups, and 402.2 eV assigning to protonated N ($–NH_3^+$), indicating that the protonation reaction between chitosan and MPA as well as MSA is an equilibrium reaction (Dambies et al. 2001; Kang et al. 2010). Figure 4G shows high resolution Au 4f spectrum of TCPPILH-4@Au NPs, and this spectrum consists of two peaks at 84.0 and 87.8 eV assigning to Au $4f_{7/2}$ and Au $4f_{5/2}$ energy levels, respectively. This is nearly identical to reported literature, indicating a metallic Au(0) state (Zhao et al. 2019a, 2019b; Zhou et al. 2018). Furthermore, after loading Au NPs, the weakness of S 2p peak (Fig. 4H) and the disappearance of protonated N (Fig. 4I) suggest the transformation of the protonated N to its neutral form and removal of some MPA and MSA, which is in accordance with the FTIR results as shown in Fig. 3. The peak of N shifts to a higher binding energy (399.4 eV) as compared to the N peak of native chitosan (399.0 eV), suggesting the interaction between the N atoms and Au NPs. Although $NaBH_4$ treatment would partially destroy the ionic interactions between chitosan and MPA/MSA during the reduction of Au^{3+} to Au NPs, the Au NPs can still be readily anchored in the TCPPILH beads through the synergistic effect of Au–S chemistry and N atoms. These integrated results reveal that the thiol groups in the hydrogel beads can be regarded as sacrificial groups. That is, although the poly(protic ionic liquids) structure is substantially destroyed in the $NaBH_4$ treatment in order to prepare Au NPs, the design of thiol-functionalized hydrogel structure contributes to the selective adsorption of Au^{3+} and thus leads to an impressive anchoring amount of Au NPs.

The thermo-stability of chitosan and TCPPILH-4 was evaluated, and the TG-DTG curves of native chitosan and TCPPILH-4 are given in Fig. S5. Different from the two-stage weight loss of native chitosan, the TCPPILH-4 sample mainly involves three decomposition stages. The first stage around 50–120 °C can be attributed to water evaporation. The second stage occurring at 195 °C of TCPPILH-4 is mainly ascribed to the degradation of PILs moieties from MPA and MSA (Zhang et al. 2020). The third stage begins from ~ 250 °C and reaches a maximum at ~ 300 °C, which is similar to the native chitosan

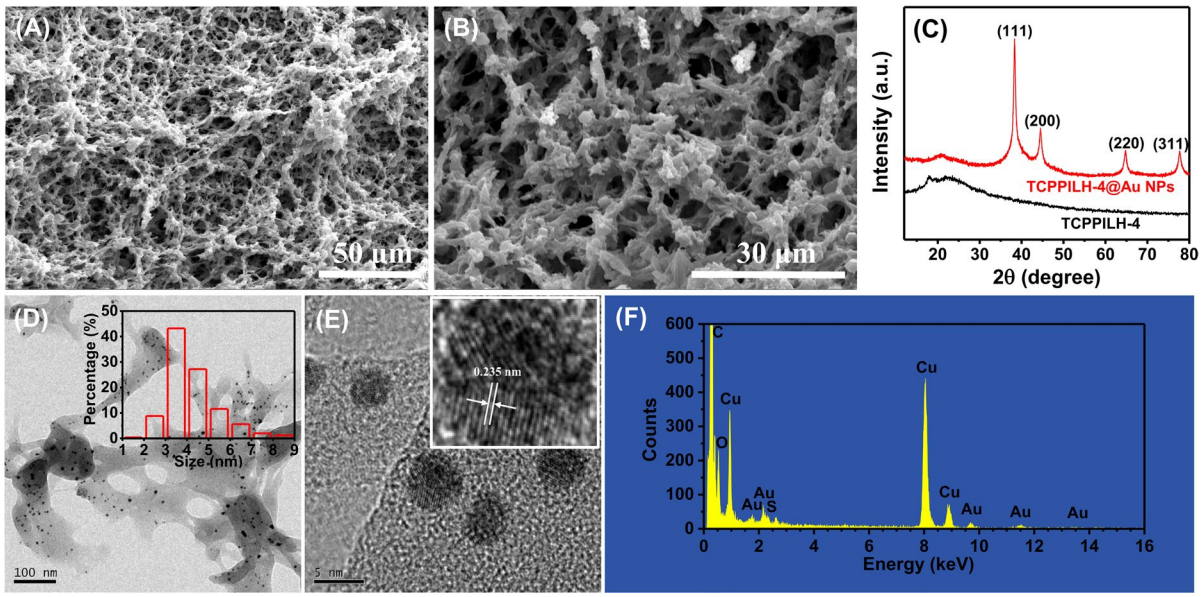

Fig. 5 **A, B** SEM images of the cross-section of TCPPILH-4@Au NPs catalysts; **C** XRD pattern, **D** TEM image (inset: the size distribution histogram), **E** HRTEM image, and **F** EDX spectrum of TCPPILH-4@Au NPs catalysts

sample; therefore, this stage can be assigned to the decomposition of chitosan chains. This difference implies decreased thermal stability for the TCPPILH-4 sample, which is in accordance with other reports on protonated chitosan structure (Wei et al. 2022; Zhang et al. 2022).

The SEM image of TCPPILH-4 shows highly porous and interconnected network structure (Fig. S6), and after anchoring Au NPs, the porous structure still remains for TCPPILH-4@Au NPs catalysts (Fig. 5A and B). The porous structure of the hydrogel is anticipated to facilitate the diffusion of the catalytic substrates through these channels. The successful anchoring of Au NPs was further confirmed by TEM (Fig. 5D and E). Obviously, the Au NPs were successfully anchored in the TCPPILH-4 beads with uniform spherical shapes, and distributed evenly without conspicuous aggregation. The average particle size of Au NPs was about 4.20 nm, determined from the size distribution histogram of Au NPs. The crystal lattice spacing of Au NPs from the HRTEM image (inset in Fig. 5E) was 0.235 nm, corresponding to the (111) faces of Au NPs (Zhao et al. 2019a, 2019b; Zhou et al. 2018). The energy dispersive X-ray spectroscopy (EDX) analysis (Fig. 5F) further indicates the presence of Au NPs. XRD pattern of TCPPILH-4@Au NPs (Fig. 5C) shows sharp diffraction peaks at 38.4, 44.5, 64.8 and 77.7°, corresponding to the (111), (200), (222) and (311) crystal plains of face-centered cubic (FCC) Au NPs, respectively (Marcelo et al. 2014; Zhao et al. 2019a, 2019b; Zhou et al. 2018). These results strongly prove the formation of Au NPs in the TCPPILH.

Catalytic application

Catalytic performance for aqueous hydrogenation of 4-NP by using TCPPILH-4@Au NPs catalysts

The catalytic performance of the TCPPILH-4@Au NPs catalysts was firstly assessed by using the catalytic hydrogenation of 4-NP to 4-AP with excess of $NaBH_4$ as a model reaction. The absorbance band at 317 nm of 4-NP solution shifts to 400 nm after addition of $NaBH_4$, and the light yellow solution changes to a bright yellow one (Fig. S7). Although the reduction of 4-NP to 4-AP by $NaBH_4$ is a thermodynamically allowed reaction, it is kinetically restricted without an efficient catalyst (Yan et al. 2018). No obvious change can be observed in the absorbance of 4-NP at 400 nm without catalysts after 2 h, indicating no hydrogenation occurred (Fig. S8). On the contrary, in the presence of TCPPILH-4@Au NPs catalysts, the hydrogenation reaction can be clearly monitored

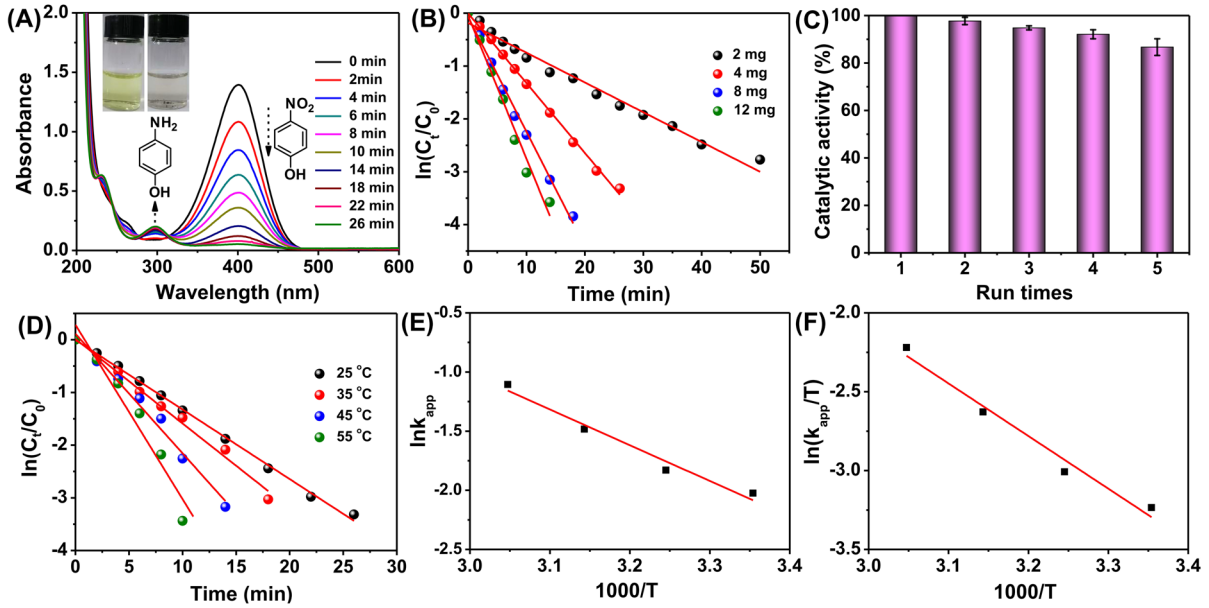

Fig. 6 **A** Time-dependent UV–vis spectra of hydrogenation of 4-NP catalyzed by the TCPPILH-4@Au NPs catalysts (4 mg) in the presence of $NaBH_4$; **B** the $\ln(C_t/C_0)$ plot versus time t with different amount of catalysts; **C** the reusability of the TCPPILH-4@Au NPs catalysts (4 mg); **D** the $\ln(C_t/C_0)$ plot versus time t with the TCPPILH-4@Au NPs catalysts (4 mg) at different temperatures; **E** the Arrhenius plot and **F** Eyring plot of the catalytic hydrogenation of 4-NP

as the gradual decrease in absorbance at 400 nm and the emergence of a new peak at 300 nm (assigned to 4-AP) with an isosbestic point at 314 nm, and the process is associated with the color change from bright yellow to colorless (Fig. 6A), indicating the efficient hydrogenation reaction of 4-NP to 4-AP catalyzed by TCPPILH-4@Au NPs catalysts.

In order to study the effect of the catalyst amount on the reaction kinetics, a series of catalytic reactions with different weight catalysts were carried out at 25 °C, as shown in Fig. 6B. The k_{app} values are calculated according to these fitted curves, as 0.056, 0.132, 0.217 and 0.271 min^{-1} for 2, 4, 8 and 12 mg catalysts (dry weight), respectively. Obviously, the k_{app} value increases with the increase in the amount of catalysts due to the availability of more catalytic sites. The TCPPILH-4@Au NPs catalysts present a high k_{app} value similar to that reported for Au NPs supported in a thioether-contained hydrogel (Ilgin et al. 2019) or in a chitosan hydrogel (Wu et al. 2015). Reusability of these TCPPILH-4@Au NPs catalysts was also investigated for five successive times in the hydrogenation of 4-NP at 25 °C. As shown in Fig. 6C, after 5 cycles, the reaction yield does not change and only 13% reduction in the activity is determined, implying the good reusability of the TCPPILH-4@Au NPs catalysts.

In order to determine E_a, $\Delta H^{\#}$, and $\Delta S^{\#}$, hydrogenation of 4-NP was carried out at 25, 35, 45 and 55 °C in the presence of TCPPILH-4@Au NPs catalysts (Fig. 6D). The k_{app} values are determined to be 0.132, 0.160, 0.227, and 0.330 min^{-1} for 25, 35, 45 and 55 °C, respectively. The $E_a = 25.14$ kJ/mol, $\Delta H^{\#} = 27.74$ kJ/mol, and $\Delta S^{\#} = -131.91$ J/(mol K) of the reduction of 4-NP are identified in the presence of TCPPILH-4@Au NPs catalysts (Fig. 6E and F). The k_{app}, E_a, recovery and recyclability reported in the literature for the catalytic reduction of 4-NP are summarized in Table S2. The k_{app} value of TCPPILH-4@Au NPs catalysts is comparable with the earlier report for the gold catalyst. However, the TCPPILH-4@Au NPs catalysts are superior to some of the different catalysts reported in the literature for the reduction of 4-NP. The k_{app} is reported as 0.043 min^{-1} for water-washed fly ash supported Fe nanoparticles (Park and Bae 2018); as 0.033 min^{-1} for peptide-based hydrogel supported Ag NPs (Paul et al. 2018); as 0.12 min^{-1} for hydrogel supported Co NPs (Sahiner et al. 2010b); and as 0.0636 min^{-1} for hydrogel supported Ni NPs (Sahiner et al. 2010a). The E_a value of TCPPILH-4@

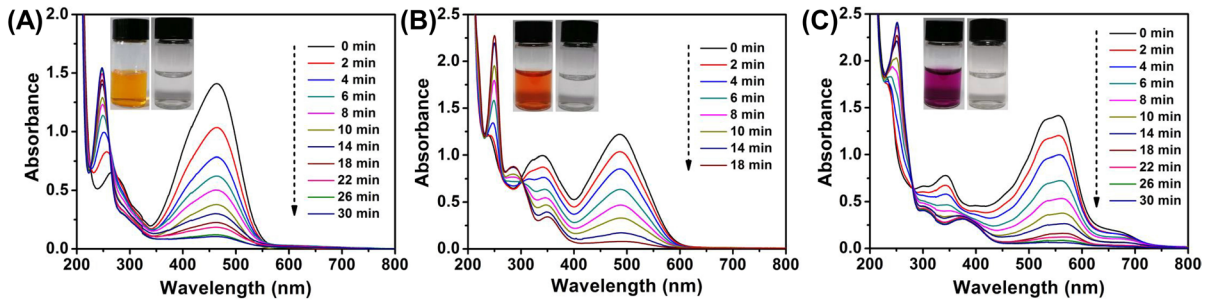

Fig. 7 Time-dependent UV–vis absorption spectra for the hydrogenation of **A** MO, **B** CR and **C** EBT catalyzed by the TCPPILH-4@Au NPs catalysts in the presence of $NaBH_4$

Au NPs catalysts complies with reported values. The E_a was reported as 38.80 kJ/mol for thioether contained hydrogel supported Au NPs (Ilgin et al. 2019); as 67.71 kJ/mol for chitosan supported Au NPs (Wu et al. 2015); as 34.8 kJ/mol for hierarchical Cu nanoparticle-aggregated cages (Jiang et al. 2018); and as 68.6 kJ/mol for silver-adsorbed waste nanocomposite (Giri et al. 2017).

Catalytic performance for aqueous hydrogenation of azo dyes by using TCPPILH-4@Au NPs catalysts

Azo dyes are typical organic pollutes in wastewater from textile industry and have caused considerable environmental problems. Thus the degradation of azo dyes in the wastewater from these industries is a one of the major tasks nowadays (Manzar et al. 2019). The azo bond (-N = N-) in the azo dyes can be cleaved through hydrogenation into nontoxic substances by Au NPs (Alle et al. 2021; Fu et al. 2019; Umamaheswari et al. 2018). Hence, three typical azo dyes, including MO, CR and EBT, were employed as pollutant models to evaluate the catalytic performance of the TCPPILH-4@Au NPs catalysts. The characteristic absorption peaks of MO (465 nm), CR (486 nm) and EBT (556 nm) decrease gradually along with the decoloration of solutions, as shown in Fig. 7, indicating the successful degradation of azo dyes. Moreover, a new absorption peak at 250 nm appears, indicating the formation of aromatic amines (Fan et al. 2009; Fu et al. 2019). From the corresponding $\ln(C_t/C_0) \sim t$ fitted curves (Fig. S9), the k_{app} values for MO, CR and EBT are determined to be 0.089, 0.149, and 0.094 min^{-1}, respectively. All these results illustrate that the TCPPILH-4@Au NPs exhibit effective catalytic performance in the degradation of azo dyes. The successful decolorization of azo dyes was reported to be related to the hydrogenation of -N = N- to -NH-NH- and then the cleavage of -NH-NH-bonds by catalytic hydrogenation (Fu et al. 2019).

Conclusion

Taking advantage of the sustainability nature and structure characteristics of chitosan as well as Au-thiol chemistry, TCPPILH was successful designed and prepared through mild protonation reaction of chitosan and MPA as well as MSA in water. The findings indicate that the materials properties and Au anchoring ability of the TCPPILH are significantly correlated with the molar ratio of MPA to MSA, and the TCPPILH shows satisfactory material properties and highest Au anchoring ability up to 151.5 mg/g when the molar ratio of MPA to MSA is set to be 2:1. Furthermore, the TCPPILH shows selective anchoring ability to Au^{3+} ions, and the outstanding performance in the Au anchoring ability is ascribed to synergetic effect of the cross-linked hydrogel network and the rich content of the thiol moieties. The as-prepared TCPPILH-4@Au NPs shows satisfactory catalytic activity and reusability in the hydrogenation of 4-NP to 4-AP, as well as hydrogenation degradation of azo dyes by using $NaBH_4$. The activation parameters of the hydrogenation of 4-NP are calculated as $E_a = 25.14$ kJ/mol, $\Delta H^{\#} = 27.74$ kJ/mol, and $\Delta S^{\#} = -131.91$ J/(mol K). In words, this work provides significant insights for the design and preparation of sustainable functional hydrogel catalytic

materials, and the as-prepared TCPPILH has great potential in the fields of green aqueous catalytic pretreatment of wastewater containing organic pollutes, Au enrichment from waste water, and so on. Related work is in progress in our lab.

Acknowledgments This work was financially supported by the National Natural Science Foundation of China (51803038, 22065007, 21774028); Science and Technology Department of Guizhou Province (Natural Science Key Fund ZK[2021]023; Platform & Talents [2016]5652, [2017]5788, [2018]5781 and [2019]5607); Science and Technology Department of Guizhou Province & Guizhou University Joint Fund ([2017]7249); and Talent Introduction Program of Guizhou University ([2017]08).

Author contribution LZ: Conceptualization, Investigation, Methodology, Writing–original draft, Funding acquisition. SF: Investigation. FH: Investigation. BL: Investigation. YL: Writing–review & editing. HS: Investigation. LH: Writing review & editing. SL: Writing–review & editing. HX: Conceptualization, Supervision, Project administration, Funding acquisition, Writing–review & editing. All authors reviewed the manuscript.

Funding This work was financially supported by the National Natural Science Foundation of China (51803038, 22065007, 21774028); Science and Technology Department of Guizhou Province (Natural Science Key Fund ZK[2021]023; Platform & Talents [2016]5652, [2017]5788, [2018]5781 and [2019]5607); Science and Technology Department of Guizhou Province & Guizhou University Joint Fund ([2017]7249); and Talent Introduction Program of Guizhou University ([2017]08).

Data availability Not applicable.

Declarations

Conflict of interest The authors declare that they have no known competing financial interests or personal relationships that could have appeared to influence the work reported in this paper.

Ethical approval This article does not contain any studies with human participants or animals performed by any of the authors.

Consent to participate This article does not contain any studies with human participants or animals performed by any of the authors.

Consent for publication The authors hereby consent to publication of the present research work in this journal, if selected for publication.

Human or animal rights Not applicable.

References

Alle M, Bandi R, Sharma G, Lee S-H, Kim J-C (2021) Shape recoverable, Au nanoparticles loaded nanocellulose foams as a recyclable catalyst for the dynamic and batch discoloration of dyes. Carbohydr Polym 258:117693. https://doi.org/10.1016/j.carbpol.2021.117693

Biswas TK, Sarkar SM, Yusoff MM, Rahman ML (2016) Synthesis and characterization of azobenzene-based gold nanoparticles for photo-switching properties. J Mol Liq 214:231–237. https://doi.org/10.1016/j.molliq.2015.12.078

Bratlie KM, Lee H, Komvopoulos K, Yang P, Somorjai GA (2007) Platinum nanoparticle shape effects on benzene hydrogenation selectivity. Nano Lett 7:3097–3101. https://doi.org/10.1021/nl0716000

Cao S, Mishra R, Pilla S, Tripathi S, Pandey MK, Shah G, Mishra AK, Prabaharan M, Mishra SB, Xin J, Pandey RR, Wu W, Pandey AC, Tiwari A (2010) Novel chitosan/gold-MPA nanocomposite for sequence-specific oligonucleotide detection. Carbohydr Polym 82:189–194. https://doi.org/10.1016/j.carbpol.2010.04.051

Castner DG, Hinds K, Grainger DW (1996) X-ray photoelectron spectroscopy sulfur 2p study of organic thiol and disulfide binding interactions with gold surfaces. Langmuir 12:5083–5086. https://doi.org/10.1021/la960465w

Chen Y, Li Y, Jiang L, Huang L, Lin Q, Chen G (2016) Fabrication of a heated electrode modified with a thiol-functionalized ionic liquid for electrochemical/electrochemiluminescence sensors. RSC Adv 6:39955–39961. https://doi.org/10.1039/C6RA05302E

Cheng J, Xu Q, Wang X, Li Z, Wu F, Shao J, Xie H (2019) Ultrahigh-surface-area nitrogen-doped hierarchically porous carbon materials derived from chitosan and betaine hydrochloride sustainable precursors for high-performance supercapacitors. Sustain Energy Fuels 3:1215–1224. https://doi.org/10.1039/C9SE00072K

Dambies L, Guimon C, Yiacoumi S, Guibal E (2001) Characterization of metal ion interactions with chitosan by X-ray photoelectron spectroscopy. Colloids Surf A 177:203–214. https://doi.org/10.1016/S0927-7757(00)00678-6

Dhakshinamoorthy A, Asiri AM, Garcia H (2017) Metal organic frameworks as versatile hosts of Au nanoparticles in heterogeneous catalysis. ACS Catal 7:2896–2919. https://doi.org/10.1021/acscatal.6b03386

Dong Y, Xiao C (2017) Formation and cleaning function of physically cross-linked dual strengthened water-soluble chitosan-based core-shell particles. Int J Biol Macromol 102:130–135. https://doi.org/10.1016/j.ijbiomac.2017.03.185

Fabre E, Murshed SMS (2021) A review of the thermophysical properties and potential of ionic liquids for thermal applications. J Mater Chem A 9:15861–15879. https://doi.org/10.1039/D1TA03656D

Fan J, Guo Y, Wang J, Fan M (2009) Rapid decolorization of azo dye methyl orange in aqueous solution by nanoscale zerovalent iron particles. J Hazard Mater 166:904–910. https://doi.org/10.1016/j.jhazmat.2008.11.091

Fu Y, Qin L, Huang D, Zeng G, Lai C, Li B, He J, Yi H, Zhang M, Cheng M, Wen X (2019) Chitosan functionalized

activated coke for Au nanoparticles anchoring: Green synthesis and catalytic activities in hydrogenation of nitrophenols and azo dyes. Appl Catal B 255:117740. https://doi.org/10.1016/j.apcatb.2019.05.042

Ge H, Hua T, Chen X (2016) Selective adsorption of lead on grafted and crosslinked chitosan nanoparticles prepared by using Pb^{2+} as template. J Hazard Mater 308:225–232. https://doi.org/10.1016/j.jhazmat.2016.01.042

Ghosh P, Rameshbabu AP, Dhara S (2014) Citrate cross-linked gels with strain reversibility and viscoelastic behavior accelerate healing of osteochondral defects in a rabbit model. Langmuir 30:8442–8451. https://doi.org/10.1021/la500698v

Giri S, Das R, van der Westhuyzen C, Maity A (2017) An efficient selective reduction of nitroarenes catalyzed by reusable silver-adsorbed waste nanocomposite. Appl Catal B 209:669–678. https://doi.org/10.1016/j.apcatb.2017.03.033

Hong M, Xu X, Wang B, Guan Z, Zheng Z, Zhang Q (2022) Polymer brush-assisted preparation of magnetic Au nanocatalyst for highly efficient reduction of organic pollutants. Colloids Surf A 639:128338. https://doi.org/10.1016/j.colsurfa.2022.128338

Huang Y, Yu H, Xiao C (2007) pH-sensitive cationic guar gum/poly (acrylic acid) polyelectrolyte hydrogels: Swelling and in vitro drug release. Carbohydr Polym 69:774–783. https://doi.org/10.1016/j.carbpol.2007.02.016

Ilgin P, Ozay O, Ozay H (2019) A novel hydrogel containing thioether group as selective support material for preparation of gold nanoparticles: synthesis and catalytic applications. Appl Catal B 241:415–423. https://doi.org/10.1016/j.apcatb.2018.09.066

Jayaramudu T, Raghavendra GM, Varaprasad K, Sadiku R, Raju KM (2013) Development of novel biodegradable Au nanocomposite hydrogels based on wheat: for inactivation of bacteria. Carbohydr Polym 92:2193–2200. https://doi.org/10.1016/j.carbpol.2012.12.006

Jiang H-L, Akita T, Ishida T, Haruta M, Xu Q (2011) Synergistic catalysis of Au@Ag core-shell nanoparticles stabilized on metal-organic framework. J Am Chem Soc 133:1304–1306. https://doi.org/10.1021/ja1099006

Jiang J, Gunasekar GH, Park S, Kim S-H, Yoon S, Piao L (2018) Hierarchical Cu nanoparticle-aggregated cages with high catalytic activity for reduction of 4-nitrophenol and carbon dioxide. Mater Res Bull 100:184–190. https://doi.org/10.1016/j.materresbull.2017.12.018

Kang J, Liu H, Zheng Y-M, Qu J, Chen JP (2010) Systematic study of synergistic and antagonistic effects on adsorption of tetracycline and copper onto a chitosan. J Colloid Interface Sci 344:117–125. https://doi.org/10.1016/j.jcis.2009.11.049

Kasaai MR, Arul J, Charlet G (2000) Intrinsic viscosity-molecular weight relationship for chitosan. J Polym Sci Part b Polym Phys 38:2591–2598. https://doi.org/10.1002/1099-0488(20001001)38:19%3c2591::AID-POLB110%3e3.0.CO;2-6

Laiho T, Leiro JA, Lukkari J (2003) XPS study of irradiation damage and different metal-sulfur bonds in dodecanethiol monolayers on gold and platinum surfaces. Appl Surf Sci 212–213:525–529. https://doi.org/10.1016/S0169-4332(03)00462-8

Laomeephol C, Ferreira H, Yodmuang S, Reis RL, Damrongsakkul S, Neves NM (2020) Exploring the gelation mechanisms and cytocompatibility of gold (III)-mediated regenerated and thiolated silk fibroin hydrogels. Biomolecules 10:466. https://doi.org/10.3390/biom10030466

Lasko CL, Pesic BM, Oliver DJ (1993) Enhancement of the metal-binding properties of chitosan through synthetic addition of sulfur- and nitrogen-containing compounds. J Appl Polym Sci 48:1565–1570. https://doi.org/10.1002/app.1993.070480908

Li X, Dong F, Zhang L, Xu Q, Zhu X, Liang S, Hu L, Xie H (2019) Cellulosic protic ionic liquids hydrogel: a green and efficient catalyst carrier for Pd nanoparticles in reduction of 4-nitrophenol in water. Chem Eng J 372:516–525. https://doi.org/10.1016/j.cej.2019.04.123

Lin S, Jiang S, Zhang Y, Dai Z, Dai Y, Xia F, Zhang X (2021) Gold nanorods crosslinking PNIPAM hydrogels via dynamic Au-thiolate interaction with stretchable, adhesive, self-healing, and photothermal properties. Gold Bull 54:59–67. https://doi.org/10.1007/s13404-021-00293-6

Liu Y, Shen X, Zhou H, Wang Y, Deng L (2016) Chemical modification of chitosan film via surface grafting of citric acid molecular to promote the biomineralization. Appl Surf Sci 370:270–278. https://doi.org/10.1016/j.apsusc.2016.02.124

Liu Y, Lin S-H, Chuang W-T, Dai N-T, Hsu S-h (2022) Biomimetic strain-stiffening in chitosan self-healing hydrogels. ACS Appl Mater Interfaces 14:16032–16046. https://doi.org/10.1021/acsami.2c01720

Luo J, Zhang N, Lai J, Liu R, Liu X (2015) Tannic acid functionalized graphene hydrogel for entrapping gold nanoparticles with high catalytic performance toward dye reduction. J Hazard Mater 300:615–623. https://doi.org/10.1016/j.jhazmat.2015.07.079

Manzar MS, Waheed A, Qazi IW, Blaisi NI, Ullah N (2019) Synthesis of a novel epibromohydrin modified crosslinked polyamine resin for highly efficient removal of methyl orange and eriochrome black T. J Taiwan Inst Chem Eng 97:424–432. https://doi.org/10.1016/j.jtice.2019.01.027

Marcelo G, López-González M, Mendicuti F, Tarazona MP, Valiente M (2014) Poly(N-isopropylacrylamide)/gold hybrid hydrogels prepared by catechol redox chemistry. characterization and smart tunable catalytic activity. Macromolecules 47:6028–6036. https://doi.org/10.1021/ma501214k

Miyamura H, Min H, Soulé J-F, Kobayashi S (2015) Size of gold nanoparticles driving selective amide synthesis through aerobic condensation of aldehydes and amines. Angew Chem Int Ed 54:7564–7567. https://doi.org/10.1002/anie.201501795

Nunes CS, Rufato KB, Souza PR, de Almeida EAMS, da Silva MJV, Scariot DB, Nakamura CV, Rosa FA, Martins AF, Muniz EC (2017) Chitosan/chondroitin sulfate hydrogels prepared in [Hmim][HSO_4] ionic liquid. Carbohydr Polym 170:99–106. https://doi.org/10.1016/j.carbpol.2017.04.073

Nutan B, Jewrajka SK (2020) PEGylated gold nanoparticles promoted rapid macromolecular chain-end transformation and formation of injectable hydrogels. J Mater Chem B 8:465–477. https://doi.org/10.1039/C9TB02001B

Park J, Bae S (2018) Formation of Fe nanoparticles on water-washed coal fly ash for enhanced reduction of p-nitrophenol. Chemosphere 202:733–741. https://doi.org/10.1016/j.chemosphere.2018.03.152

Paul S, Basu K, Das KS, Banerjee A (2018) Peptide-based hydrogels as a scaffold for in situ synthesis of metal nanoparticles: catalytic activity of the nanohybrid system. ChemNanoMat 4:882–887. https://doi.org/10.1002/cnma.201800227

Qian W, Texter J, Yan F (2017) Frontiers in poly(ionic liquid)s: syntheses and applications. Chem Soc Rev 46:1124–1159. https://doi.org/10.1039/C6CS00620E

Sahiner N, Ozay H, Ozay O, Aktas N (2010a) New catalytic route: hydrogels as templates and reactors for in situ Ni nanoparticle synthesis and usage in the reduction of 2- and 4-nitrophenols. Appl Catal A 385:201–207. https://doi.org/10.1016/j.apcata.2010.07.004

Sahiner N, Ozay H, Ozay O, Aktas N (2010b) A soft hydrogel reactor for cobalt nanoparticle preparation and use in the reduction of nitrophenols. Appl Catal B 101:137–143. https://doi.org/10.1016/j.apcatb.2010.09.022

Shi S, Zhang L, Wang T, Wang Q, Gao Y, Wang N (2013) Poly(N-isopropylacrylamide)-Au hybrid microgels: synthesis, characterization, thermally tunable optical and catalytic properties. Soft Matter 9:10966–10970. https://doi.org/10.1039/C3SM52303A

Singh SK, Savoy AW (2020) Ionic liquids synthesis and applications: an overview. J Mol Liq 297:112038. https://doi.org/10.1016/j.molliq.2019.112038

Tabassum N, Ahmed S, Ali MA (2021) Chitooligosaccharides and their structural-functional effect on hydrogels: a review. Carbohydr Polym 261:117882. https://doi.org/10.1016/j.carbpol.2021.117882

Tan X, Wang G, Zhong L, Xie F, Lan P, Chi B (2021) Regeneration behavior of chitosan from ionic liquid using water and alcohols as anti-solvents. Int J Biol Macromol 166:940–947. https://doi.org/10.1016/j.ijbiomac.2020.10.251

Thoniyot P, Tan MJ, Karim AA, Young DJ, Loh XJ (2015) Nanoparticle-hydrogel composites: concept, design, and applications of these promising, multi-functional materials. Adv Sci 2:1400010. https://doi.org/10.1002/advs.201400010

Umamaheswari C, Lakshmanan A, Nagarajan NS (2018) Green synthesis, characterization and catalytic degradation studies of gold nanoparticles against congo red and methyl orange. J Photochem Photobiol B 178:33–39. https://doi.org/10.1016/j.jphotobiol.2017.10.017

Ventura-Espinosa D, Martín S, García H, Mata JA (2021) Ligand effects in the stabilization of gold nanoparticles anchored on the surface of graphene: implications in catalysis. J Catal 394:113–120. https://doi.org/10.1016/j.jcat.2020.12.027

Wang T, Song Y, Jin L, Li J, Gao Y, Shi S (2017) Assembly of preformed gold nanoparticles onto thermoresponsive poly(N-isopropylacrylamide)-based microgels on the basis of Au-thiol chemistry. Chin J Chem 35:1755–1760. https://doi.org/10.1002/cjoc.201700287

Wang Q, Chen L, Liu Z, Tsumori N, Kitta M, Xu Q (2019) Phosphate-mediated immobilization of high-performance AuPd nanoparticles for dehydrogenation of formic acid at room temperature. Adv Funct Mater 29:1903341. https://doi.org/10.1002/adfm.201903341

Wei W, Chen W (2012) "Naked" Pd nanoparticles supported on carbon nanodots as efficient anode catalysts for methanol oxidation in alkaline fuel cells. J Power Sources 204:85–88. https://doi.org/10.1016/j.jpowsour.2012.01.032

Wei BX, Zou J, Pu QQ, Shi K, Xu BG, Ma YK (2022) One-step preparation of hydrogel based on different molecular weights of chitosan with citric acid. J Sci Food Agric 102:3826–3834. https://doi.org/10.1002/jsfa.11732

Wu X-Q, Wu X-W, Huang Q, Shen J-S, Zhang H-W (2015) In situ synthesized gold nanoparticles in hydrogels for catalytic reduction of nitroaromatic compounds. Appl Surf Sci 331:210–218. https://doi.org/10.1016/j.apsusc.2015.01.077

Wu Z, Zhou W, Deng W, Xu C, Cai Y, Wang X (2020) Antibacterial and hemostatic thiol-modified chitosan-immobilized AgNPs composite sponges. ACS Appl Mater Interfaces 12:20307–20320. https://doi.org/10.1021/acsami.0c05430

Yan Z, Fu L, Zuo X, Yang H (2018) Green assembly of stable and uniform silver nanoparticles on 2D silica nanosheets for catalytic reduction of 4-nitrophenol. Appl Catal B 226:23–30. https://doi.org/10.1016/j.apcatb.2017.12.040

Yan P, Zhang X, Wang X, Zhang X (2020) Controllable preparation of monodisperse mesoporous silica from microspheres to microcapsules and catalytic loading of Au nanoparticles. Langmuir 36:5271–5279. https://doi.org/10.1021/acs.langmuir.0c00629

Zhang N, Zhang H, Li R, Xing Y (2020) Preparation and adsorption properties of citrate-crosslinked chitosan salt microspheres by microwave assisted method. Int J Biol Macromol 152:1146–1156. https://doi.org/10.1016/j.ijbiomac.2019.10.203

Zhang W, Jiang Q, Shen J, Gao P, Yu D, Xu Y, Xia W (2022) The role of organic acid structures in changes of physicochemical and antioxidant properties of crosslinked chitosan films. Food Packag Shelf Life 31:100792. https://doi.org/10.1016/j.fpsl.2021.100792

Zhao Y, Zhang X, Wang Y, Wu Z, An J, Lu Z, Mei L, Li C (2014) In situ cross-linked polysaccharide hydrogel as extracellular matrix mimics for antibiotics delivery. Carbohydr Polym 105:63–69. https://doi.org/10.1016/j.carbpol.2014.01.068

Zhao L, Wang Y, Li Z, Deng Y, Zhao X, Xia Y (2019a) Facile synthesis of chitosan-gold nanocomposite and its application for exclusively sensitive detection of Ag^{+} ions. Carbohydr Polym 226:115290. https://doi.org/10.1016/j.carbpol.2019.115290

Zhao M, Zhao J, Huang Z, Wang S, Zhang L (2019b) One pot preparation of magnetic chitosan-cystamine composites for selective recovery of Au(III) from the aqueous solution. Int J Biol Macromol 137:721–731. https://doi.org/10.1016/j.ijbiomac.2019.07.022

Zhao MH, Li XT, Huang Z, Wang SX, Zhang LB (2021) Facile cross-link method to synthesize chitosan-based adsorbent with superior selectivity toward gold ions: batch and column studies. Int J Biol Macromol 172:210–222. https://doi.org/10.1016/j.ijbiomac.2021.01.046

Zhou X, Zhao G, Chen M, Gao W, Zhou X, Xie X, Yang L, Du G (2018) Facile and green approach to prepare nanostructured Au@MnO_2 and its applications for catalysis and fluorescence sensing of glutathione in human blood. ACS Sustain Chem Eng 6:3948–3956. https://doi.org/10.1021/acssuschemeng.7b04313

Zhu J, Zhang X, Qin Z, Zhang L, Ye Y, Cao M, Gao L, Jiao T (2021) Preparation of PdNPs doped chitosan-based composite hydrogels as highly efficient catalysts for reduction of 4-nitrophenol. Colloids Surf A 611:125889. https://doi.org/10.1016/j.colsurfa.2020.125889

Zubair Iqbal M, Ali I, Khan WS, Kong X, Dempsey E (2021) Reversible self-assembly of gold nanoparticles in response to external stimuli. Mater Des 205:109694. https://doi.org/10.1016/j.matdes.2021.109694